Atmos. Chem. Phys. Discuss., 10, 22019–22046, 2010
www.atmos-chem-phys-discuss.net/10/22019/2010/
doi:10.5194/acpd-10-22019-2010

Atmospheric Chemistry and Physics Discussions

Tropospheric temperature response to stratospheric ozone recovery in the 21st century

Y. Hu[1], **Y. Xia**[1], **and Q. Fu**[2]

[1]Dept. of Atmospheric and Oceanic Sciences, School of Physics, Peking University, Beijing, 100871, China
[2]Dept. of Atmospheric Sciences, University of Washington, Seattle, WA, 98195-1640, USA

Received: 26 July 2010 – Accepted: 18 August 2010 – Published: 22 September 2010

Correspondence to: Y. Hu (yyhu@pku.edu.cn)

Published by Copernicus Publications on behalf of the European Geosciences Union.

Abstract

Observations show a stabilization or a weak increase of the stratospheric ozone layer since the late 1990s. Recent coupled chemistry-climate model simulations predicted that the stratospheric ozone layer will likely return to pre-1980 levels in the middle of the 21st century, as a results of the decline of ozone depleting substances under the 1987 Montreal Protocol. Since the ozone layer is an important component in determining stratospheric and tropospheric-surface energy balance, the recovery of the ozone layer may have significant impact on tropospheric-surface climate. Here, using multi-model ensemble results from both the Intergovernmental Panel on Climate Change Fourth Assessment Report (IPCC-AR4) models and coupled chemistry-climate models, we show that as ozone recovery is considered, the troposphere is warmed more than that without considering ozone recovery, suggesting an enhancement of tropospheric warming due to ozone recovery. It is found that the enhanced tropospheric warming is mostly significant in the upper troposphere, with a global mean magnitude of ~0.41 K for 2001–2050. We also find that relatively large enhanced warming occurs in the extratropics and polar regions in summer and autumn in both hemispheres while the enhanced warming is stronger in the Northern Hemisphere than in the Southern Hemisphere. Enhanced warming is also found at the surface. The strongest enhancement of surface warming is located in the Arctic in boreal winter. The global annual mean enhancement of surface warming is about 0.16 K for 2001–2050.

1 Introduction

After about 20 years of severe depletion from the late 1970s to late 1990s (Solomon, 1999), the stratospheric ozone layer shows a stabilization or a weak increase in the past decade, consistent with the observed decline in ozone depleting substances (ODSs) that peaked in the middle 1990s (Weatherhead and Andersen, 2006; WMO, 2007). Since ODSs are also greenhouse gases, the reduction of ODSs under the 1987 Montreal Protocol serves to protect both the ozone layer and climate (Velders et al., 2007). Coupled chemistry-climate model (CCM) simulations, with projected

ACPD
10, 22019–22046, 2010

stratospheric chlorine loading, predicted that stratospheric ozone will return to pre-1980 levels around 2050 and may even be above pre-1980 levels by 2100 (Weatherhead and Andersen, 2006; WMO, 2007; Eyring et al., 2007; Chipperfield, 2009). The recovery of the ozone layer will not only help reduce ultraviolet transmission, which benefits ecosystems on the Earth's surface, but also have important impacts on troposphere climate throughout its radiative effect.

The radiative effect of the ozone layer is an important component in determining the energy balance in the troposphere and surface (Ramanathan and Dickinson, 1979). While ozone warms the stratosphere by absorbing solar radiation and thermal infrared radiation emitted from the troposphere and surface, its emission in the 9.6 µm band cools the stratosphere but warms the troposphere. Because the ozone layer absorbs more radiative energy than it emits, an increase (decrease) of stratospheric ozone increases (decreases) stratospheric temperatures, and also increases (decreases) the downward infrared radiation to the troposphere, causing tropospheric warming (cooling) (Ramanathan and Dickinson, 1979). The radiative forcing of ozone layer changes, especially stratospheric ozone depletion in the last 20 years of the 20th century, and its impact on troposphere-surface temperatures had been investigated using radiation transfer models (Wang et al., 1980, 1991; Lacis et al., 1990; Forster and Shine, 1997), general circulation model (GCM) (Ramaswamy et al., 1992), and satellite observations (Molnar et al., 1994). All these studies indicated that stratospheric ozone depletion caused a significant negative radiative forcing on the troposphere, which may have offset up to 30% of the positive forcing due to increasing well-mixed greenhouse gases between the late 1970s and the late 1990s. In a more recent study, Cordero and Forster (2006) showed that GCMs with stratospheric ozone depletion yielded weaker warming trends compared with GCMs without ozone depletion in IPCC-AR4 20th century simulations. They showed that the difference of warming trends in the upper troposphere is about 0.4 K over 1950–1999 and 0.2 K over 1979–1999.

Because of the latitudinal dependence of the ozone layer, changes in stratospheric ozone would cause changes in latitudinal thermal structures in the troposphere

ACPD
10, 22019–22046, 2010

(Ramanathan and Dickinson, 1979). Studies in the past decade have demonstrated evidence that ozone depletion had caused changes in tropospheric circulations and wave activity (Hartmann et al., 2000; Thompson and Solomon, 2002; Hu and Tung, 2003; Chen and Held, 2009). It was shown that stratospheric ozone depletion from the late 1970s to the late 1990s have caused accelerated westerly winds and decreased wave activity at middle and high latitudes. The accelerated westerly winds near the surface consequently cause surface warming over the Antarctic Peninsula (Thompson and Solomon, 2002) and European-Asian continents regions (Hartmann et al., 2002; Thompson and Wallace, 2001; Hu et al., 2005).

On the other hand, a positive radiative forcing associated with ozone recovery is expected in the 21st century, and that the changes in atmospheric circulations mentioned above will be reversed. Using a coupled chemistry-climate model (CCM), Perlwitz et al. (2008) have shown that the recovery of the Antarctic ozone hole will lead to a trend toward the negative polarity of the southern annular mode (SAM) in austral summer, and that the negative SAM trend forced by ozone recovery dominates and opposes that induced by increasing greenhouse gases. Based on multi-model ensemble comparison of IPCC-AR4 GCM results for the 21st century and CCM results, Son et al. (2008, 2009a, 2010) have examined the influences of the recovery of the Antarctic ozone hole on Southern-Hemisphere (SH) troposphere-surface climate. They showed nearly the same results as those in Perlwitz et al. (2008).

The main goal of the present study is to demonstrate that ozone recovery may have important impacts on troposphere-surface climate over the globe, not only at SH high latitudes. We will show that stratospheric ozone recovery may actually have greater impacts on tropospheric climate in the Northern Hemisphere (NH) than in SH. We will focus on tropospheric temperature response to the radiative forcing associated with ozone recovery by comparing temperature trends from three groups of simulations for the 21st century. The model data used here is described in Sect. 2. Results will be presented in Sect. 3. Discussion and conclusions are summarized in Sect. 4.

ACPD
10, 22019–22046, 2010

2 Simulation data and methods

The data used in this study are from IPCC-AR4 simulations for the 21st century with the A1B scenario for greenhouse gases (IPCC, 2007) and simulations from the first version of CCM validation (CCMVal-1) models for the Stratospheric Processes And their Role in Climate project (SPARC) (Eyring et al., 2006). The IPCC-AR4 models are separated into 2 groups, depending on whether a model has prescribed ozone recovery (see Table 1). Therefore, there are three groups of models: 11 IPCC-AR4 models without ozone recovery, 10 IPCC-AR4 models with prescribed ozone recovery, and 8 CCMVal-1 models (Table 2). Hereafter, the three groups of models are denoted as AR4-NO-O_3, AR4-O_3, and CCMVal-1, respectively. In temperature trend calculations, all available ensemble members are used for each model.

The prescribed ozone recovery in AR4-O_3 models is either considered as a linear function of time or from the predictions of two-dimensional models which are forced by halogen loading based on the Montreal Protocol (Meehl et al., 2007). CCMVal-1 models are all integrated up to the year 2050 and are forced with the IPCC A1B scenario for greenhouse gases, Ab scenario for halogen concentrations and prescribed sea surface temperatures (SST) from their own AR4 coupled atmosphere-ocean model simulations that have prescribed ozone recovery, except for MRI which is forced with SSTs from coupled simulations without including prescribed ozone recovery (Eyring et al., 2006). In contrast to AR4 models, CCMVal-1 models have fully interactive stratospheric chemistry and well-resolved stratospheres with better parameterizations of gravity-wave drags. Regardless of the details, the major difference in external forcing between AR4-NO-O_3 and other two groups of models is that the latter two include ozone recovery.

Although these models may have different internal processes and simulation performances, previous studies by comparing AR4-O_3/CCMVal-1 with AR4-NO-O_3 results showed a consistent result, that is, the recovery of the Antarctic ozone hole causes the weakening of the southern polar night jet and negative trends in SAM (Perlwizt et al.,

ACPD
10, 22019–22046, 2010

2008; Son et al., 2008, 2009a, 2010). More importantly, the mean transient climate sensitivity of the AR4-NO-O_3 models is the same as that from the AR4-O_3 models, which is 1.7 °C (IPCC, 2007). Therefore, these simulations offer an opportunity to evaluate tropospheric temperature response to the radiative forcing associated with ozone recovery. Since all CCMVal-1 models are forced with the A1B scenario of greenhouse gases, we only use AR4 output with the A1B scenario. Comparison of temperature trends are shown for the period of 2001–2050 because almost all CCMVal-1 models and two-dimensional chemistry models predicted that ozone will linearly return to pre-1980 levels around 2050 (Weatherhead and Andersen, 2006; Eyring et al., 2007; WMO, 2007), and ozone recovery in AR4-O_3 models is also linearly prescribed over the same period (Meehl et al., 2007). Linear trends in monthly temperatures are calculated from the ensemble average for each model, and the trends are averaged over all models for each group of models.

3 Results

Figure 1a shows vertical profiles of global annual mean temperature trends over 2001–2050 for the three groups of models. All predict warming in the troposphere and lower stratosphere but cooling at higher stratospheric layers. The maximum warming is around 300 hPa. The warming is caused by increasing well-mixed greenhouse gases in all models (WMO, 2007; IPCC, 2007) and also partly by stratospheric ozone increase in AR4-O_3 and CCMVal-1 models as addressed below.

Figure 1a also demonstrates differences in tropospheric trends between AR4-NO-O_3 models and the other two model groups, which is our key interest in this paper. The warming trends in AR4-O_3 and CCMVal-1 models show high consistency in the troposphere and are all greater than that in AR4-NO-O_3 models. The largest difference in tropospheric warming trends is around 300 hPa, which is about 0.41 K over the 50 years between AR4-O_3 and AR4-NO-O_3 and also between CCMVal-1 and AR4-NO-O_3. It is about one-fifth of the averaged warming trends over all models at 300 hPa, which is about 2.0 K for the 50 years. The stronger warming indicates that the tropospheric

ACPD
10, 22019–22046, 2010

warming due to the increase of greenhouse gases will be enhanced by stratospheric ozone recovery.

To further illustrate tropospheric temperature responses to the radiative forcing of stratospheric ozone changes, we also calculate temperature trends during the period 1965–1999 when the ozone layer was depleted, using the AR4 and CCMVal-1 simulation results for the 20th century. In general, AR4 models with prescribed ozone recovery for 21st century simulations also have prescribed ozone depletion for 20th century simulations. Among AR4 models for 20th century simulations, 14 models have prescribed ozone depletion, and 9 models do not (see Table 1). Among the 8 CCMVal-1 models, five have the 20th century simulations starting from 1960, and the other three started from 1980. Thus, data from these 5 CCMVal-1 models are used here (see Table 2).

Temperature trends over 1965–1999 are shown in Fig. 1b. It is evident that both AR4 models with ozone depletion and CCMVal-1 models produced weaker tropospheric warming compared with AR4 models without ozone depletion. The trend difference at 300 hPa between AR4 models with and without ozone depletion is about −0.26 K over the 35 years. The trend difference between CCMVal-1 models and AR4 models without ozone depletion is larger, about −0.36 K over the 35 years. Previous work reported that the temperature trend difference between AR4 models with and without ozone depletion is about −0.4 K over 1958–1999 and −0.2 K over 1979–1999, respectively (Cordero and Forster, 2006). It appears that the enhanced tropospheric warming associated with ozone recovery is comparable to the reduced warming by ozone depletion.

Annual and regional mean temperature trends are plotted in Fig. 2. In all regions, both AR4-O_3 and CCMVal-1 models display greater tropospheric warming trends compared with AR4-NO-O_3 models. In particular, trend differences in the Antarctic (Fig. 2a), NH middle latitudes (Fig. 2e), and the Arctic (Fig. 3f) are larger than in other regions. In the Antarctic and NH middle latitudes, CCMVal-1 models shows greater tropospheric warming than that generated by AR4-O_3 models, while in other regions, the two groups

ACPD
10, 22019–22046, 2010

of models have almost the same warming magnitudes. Annual and hemispheric mean temperature trends are plotted in Fig. 3. One can find that tropospheric trend differences are larger in NH than in SH, and again that the largest differences are at 300 hPa. In NH, the largest trend differences at 300 hPa between AR4-O3 and AR4-NO-O3 models and between CCMVal-1 and AR4-NO-O3 models are very close, about 0.47 K and 0.49 K over the 50 years, respectively. In SH, they are about 0.33 K and 0.32 K, respectively. Thus, enhanced warming at 300 hPa is about 0.15 K greater in NH than in SH.

To show vertical and latitudinal distribution of tropospheric temperature responses to ozone recovery in more detail, we plot vertical cross-sections of annual and zonal mean temperature trends for the three groups of models in Fig. 4. First, these plots show similar spatial trend patterns, with maximum warming all in the tropical upper troposphere which is a common feature in all GCMs (IPCC, 2007). A band of relatively large warming trends extends from the tropical upper troposphere to the NH upper troposphere and to the NH high-latitude surface. Second, Fig. 4b and c all show differences from Fig. 4a. In the stratosphere, both Fig. 4b and c show warming trends in polar regions, especially in the Antarctic, in contrast to the cooling trends in Fig. 4a. It is indicative of the radiative warming effect of ozone recovery in stratospheric polar regions. In the troposphere, warming trends in Fig. 4b and c are all greater than in Fig. 4a. In particular, the band of relatively large warming trends in the tropical and NH upper troposphere in Fig. 4b and c are greater than that in Fig. 4a.

Differences of temperature trends between AR4-O_3/CCMVal-1 and AR4-NO-O_3 models are plotted in Fig. 5a and b, respectively. Both plots show dominant positive trend differences in the troposphere, indicating enhanced tropospheric warming associated with ozone recovery. They also show similar spatial patterns. That is, enhanced warming is stronger in the middle and upper troposphere than at lower levels, and enhanced warming is stronger in NH than in SH. In Fig. 5a, the maximum enhanced warming is located in the Arctic upper troposphere, about 0.75 K over 2010–2050. In Fig. 5b, the maximum enhanced warming is near the Arctic surface, about 1.0 K.

ACPD
10, 22019–22046, 2010

The spatial patterns of tropospheric temperature trend differences in Fig. 5 resemble those of tropospheric warming trends (Fig. 4), indicating that the enhanced warming is not due to model performance. There are several likely reasons that are responsible for the stronger enhanced warming in the tropical and extratropical upper troposphere. In the tropical region, the increased warming in the upper troposphere is partly related to the moist adiabatic process (IPCC, 2007). It may also be partly due to the absorption of increased ozone emission at 9.6 μm by tropospheric high clouds and absorption of increased downward infrared radiation of stratospheric greenhouse gas (e.g., CO_2 and H_2O) emission by the upper troposphere. It was shown, using radiative-convective models, that about 50% downward infrared radiation of stratospheric ozone is absorbed by tropospheric high clouds, and that most downward infrared radiation from stratospheric greenhouse gases is absorbed in the upper troposphere (Ramanathan and Dickinson, 1979). In addition to contributing to enhanced warming in the upper troposphere, the increase in downward longwave radiation from ozone recovery may also contribute to the enhanced warming maxima near the tropical tropopause from between 70 and 150 hPa in both Fig. 5a and b (Forster et al., 2007).

Figure 5a and b for the stratosphere show both similarity and differences. The similarity is the large enhanced warming in the polar regions, especially in the Antarctic lower stratosphere. This is because ozone depletion is more severe in both polar regions than at lower latitudes from the late 1970s to the late 1990s (Solomon, 1999), and ozone recovery implies more ozone increases in the polar stratosphere and, thus, stronger warming. The difference is that Fig. 5b shows negative values in the stratosphere, indicating stronger cooling trends in CCMVal-1 models compared with AR4-NO-O_3 models. This was attributed to both a weak decrease in ozone and increased upwelling in the tropical lower stratosphere in CCMVal-1 models (Son et al., 2009b).

Enhanced tropospheric warming has seasonal variations. Since both Fig. 1a and Fig. 5 indicate that the largest enhanced tropospheric warming is in the upper troposphere, we focus on seasonal variations of temperature trends and their differences at 300 hPa. Figure 6 shows latitude-month plots of temperature trends at 300 hPa for

ACPD
10, 22019–22046, 2010

the three model groups. The common feature in the three plots is that they all show larger warming trends in the tropics than at higher latitudes, and that the larger warming trends extend from the tropics to NH middle and high latitudes in boreal summer. The differences are that warming trends are generally greater in both AR4-O_3 and CCMVal-1 models than in AR4-NO-O_3 models, and that both AR4-O_3 and CCMVal-1 models show larger warming trends at SH middle and high latitudes in austral summer than in other seasons.

Differences between Fig. 6b and a and between Fig. 6c and a are illustrated in Fig. 7a and b, respectively. First, both plots demonstrate dominant enhanced warming over the globe. Second, both plots show stronger enhanced warming in the extratropics and polar regions in summer and autumn for both hemispheres. The temporal and spatial patterns of enhanced warming in the extratropics and polar regions resemble that of temperature trends (Fig. 6). Trend differences between CCMVal-1 and AR4-NO-O_3 models have two maxima (Fig. 7b). One is located in the NH extratropics in boreal summer, and the other is in the Antarctic in austral summer. Both maxima have much greater values compared with that in Fig. 7a, indicating different tropospheric temperature responses to prescribed and interactive ozone recovery. The maximum difference in the NH extratropics in Fig. 7b is up to 1.50 K for the 50 years, and that in the Antarctic it is greater than 3.0 K. While the seasonal and latitudinal variations of enhanced warming are qualitatively consistent with results from radiative-convective models (Ramanathan and Dickinson, 1979; Forster and Shine, 1997), it is unknown what caused such large enhanced warming in the NH extratropics in boreal summer.

Comparison of seasonal and regional mean temperature trends at 300 hPa are shown in Fig. 8. For all four seasons, as shown above, both AR4-O_3 and CCMVal-1 models produce larger warming trends than AR4-NO-O_3 models do. For March-April-May (MAM) and September-October-November (SON) (Fig. 8a and c), warming trends in AR4-O_3 and CCMVal-1 models are comparable at all latitudes in general, and they all show larger differences from the trends in AR4-NO-O_3 models in NH than in SH. For boreal summer (Fig. 8b), CCMVal-1 models yield the largest warming trend at NH

ACPD
10, 22019–22046, 2010

middle latitudes, about 3.1 K for the 50 years, while in SH warming trends are larger in AR4-O_3 models than in CCMVal-1 models. For austral summer (Fig. 8d), warming trends are larger in CCMVal-1 models than in AR4-O_3 models at all latitudes. Especially in the Antarctic, the largest warming trend in CCMVal-1 models is about 3.0 K over the 50 years, nearly double of the warming trend in AR4-O_3 models.

Near-surface air temperatures also demonstrate enhanced warming associated with ozone recovery, which can be seen in Figs. 1–3. To show near-surface air temperature responses to ozone recovery, we calculate surface air temperature (SAT) trends for the two groups of AR4 models and their differences (CCMVal-1 models have no available SAT output). Figure 9a and b show latitude-month plots of SAT trends from AR4-NO-O_3 and AR4-O_3 models, respectively. Both groups of models display dominant global warming trends. They also show similar seasonal-spatial patterns of SAT trends. That is, warming trends are greater in NH than in SH, and stronger warming trends are in polar regions in winter than in other regions for both hemispheres, especially in the Arctic in boreal winter. Overall, the SAT trends in AR4-O_3 models are generally greater than in AR4-NO-O_3 models.

Trend differences between AR4-O_3 and AR4-NO-O_3 models are shown in Fig. 10. Enhanced warming is dominant, except for the austral winter and spring over Antarctic. Maximum enhanced warming is found in the Arctic in boreal autumn and winter. At NH middle latitudes, large enhanced warming occurs in boreal summer. In SH, trend differences in the tropics and extratropics have no seasonal variations. Again, the temporal and spatial patterns of trend differences resemble that of SAT trends (Fig. 9), both indicating the polar amplification in the Arctic due to the ice-albedo feedback (IPCC, 2007). It is worth pointing out that the negative differences in the Antarctic in austral winter and spring are mainly due to weaker warming over the western Antarctic, including the Antarctic Peninsula, in AR4-O_3 models. This is contrasted to observed SAT warming over the same region for the period of 1969–2000 (Thompson and Solomon, 2002), which was suggested as a result of ozone depletion in the Antarctic stratosphere (Thompson and Solomon, 2002; Gillett and Thompson, 2003). Therefore, the

ACPD
10, 22019–22046, 2010

contrast suggests that ozone recovery may dominate and offset greenhouse warming over the western Antarctic (Perlwitz et al., 2008). The global and annual average of enhanced SAT warming is about 0.16 K during 2001–2050. The enhanced SAT warming has large asymmetry between the two hemispheres. The annual and hemispheric enhanced warming is 0.35 K in NH and 0.11 K in SH for the 50 years.

4 Discussion and conclusions

By comparing multimodel ensemble simulations, we have demonstrated that tropospheric and surface temperatures have robust responses to stratospheric ozone recovery in the 21st century. Both AR4 models with prescribed ozone recovery and coupled chemistry-climate models with projected reduction of atmospheric chlorine loading all predict highly consistent enhanced warming in the troposphere compared with AR4 models without ozone recovery. For global and annual average, the maximum enhanced warming is located in the upper troposphere, with a value of about 0.41 K for the period of 2001–2050, and enhanced SAT warming is about 0.16 K. The enhanced tropospheric warming displays asymmetry between the two hemispheres. Both AR4 models with ozone recovery and CCMVal-1 models yield stronger enhanced warming in NH than in SH, about 0.48 K versus about 0.33 K at 300 hPa for the 50 years. The enhanced SAT warming is about 0.35 K in NH, contrasted to 0.11 K in SH. Enhanced tropospheric and surface warming also shows seasonal and latitudinal variations. In the upper troposphere, relatively large enhanced warming occurs in polar regions and middle latitudes in summer for both hemispheres. On the surface, relatively large enhanced warming occurs in polar regions in winter for both hemispheres, especially in the Arctic. Relatively large enhanced surface warming also occurs in NH middle latitudes in summer.

The results here suggest that the positive radiative forcing associated with ozone recovery will play an important role in global climate change in the 21st century. The non-uniform enhancement of tropospheric warming may alter tropospheric circulations and regional as well as global climate. The greater enhanced warming in the upper

ACPD
10, 22019–22046, 2010

troposphere than at lower levels suggests an increase in atmospheric stability in the troposphere, causing weakened convection. The greater enhancement at middle and high latitudes in summer for both hemispheres indicates weakened latitudinal temperature gradients and, thus, weakened baroclinic wave activity and storm tracks in the extratropics. In particular, enhanced tropospheric warming in polar regions will lead to reversed polarity of the annular mode (Perlwitz et al., 2008; Son et al., 2008, 2009a, 2010). The enhanced SAT warming, especially the relatively large enhancement in the Arctic autumn and winter, may accelerate sea-ice melting in Arctic Ocean.

It should be noted that the results here are based on the moderate emission scenario of greenhouse gases (A1B scenario). High emission scenarios of greenhouse gases, such as A2 scenario, will lead to stronger stratospheric cooling, which would consequently cause greater increases in stratospheric ozone (WMO, 2007) or even supper-ozone recovery (Chipperfield, 2009). In this case, the enhanced troposphere-surface warming would be even greater.

Since AR4 models have no well-documented prescription of ozone recovery (Son et al., 2008), we are unable to directly calculate downward infrared radiation from the stratosphere to the troposphere associated with ozone recovery and to compare it with the radiative forcing of ozone in CCMVal-1 models. Therefore, the results shown here do not directly show that the enhanced tropospheric and surface warming is caused by the radiative forcing due to ozone recovery alone. But we show the strong evidence that it is by noticing the positive feedbacks in amplifying the radiative forcing associated with ozone recovery on tropospheric and surface warming. That is, the temporal and spatial patterns of enhanced tropospheric and surface warming trends resemble that of tropospheric warming trends, with relatively large enhanced warming occurring in the places where warming trends are relatively large in general, such as the upper troposphere, NH middle latitudes in summer, and the Arctic surface in winter. It is known that the relatively large warming trends in the upper troposphere in GCM simulations are due to positive lapse-rate water-vapour feedback (IPCC, 2007), and that relatively strong warming on the Arctic surface are due to positive ice-albedo feedback.

ACPD
10, 22019–22046, 2010

The results reported here are based on multimodel ensemble averages. In future studies, it will also be useful to examine tropospheric and surface temperature responses to stratospheric ozone recovery with an individual CCM, which would reduce effects due to different model performances. In addition, CCMVal-1 models all used prescribed SSTs from AR4-O_3 models. It may partly or largely damp tropospheric and surface temperature responses to the radiative forcing of ozone recovery. Thus, coupled atmospheric-oceanic CCM simulations are necessary for future studies and for the next IPCC report.

Acknowledgements. We acknowledge the modelling groups, the Program for Climate Model Diagnosis and Intercomparison (PCMDI), and the WCRP Working Group on Coupled Modelling (WGCM) for their roles in making available the WCRP CMIP3 multi-model dataset. Support of this dataset is provided by the Office of Science, US Department of Energy. We thank the World Climate Research Program SPARC CCMVal-1 project for organizing the chemistry-climate model (CCM) data analysis activity, the British Atmospheric Data Centre for collecting and archiving the CCM output. This project is supported by the National Basic Research Program of China (973 Program, 2010CB428606) and by NSF of China under grant 40875042. Q. Fu is also in part supported by NOAA Grant NA08OAR4310725.

References

Chen, G. and Held, I. M.: Phase speed spectra and the recent poleward shift of Southern Hemisphere surface westerlies. Geophys. Res. Lett., 34, L21805, doi:10.1029/2007GL031200, 2007.

Chipperfield, M.: Nitrous oxide delays ozone recovery, Nature Geoscience, 2, 742–743, 2009.

Cordero, E. C. and Forster, P. M. de F.: Stratospheric variability and trends in models used for the IPCC AR4, Atmos. Chem. Phys., 6, 5369–5380, doi:10.5194/acp-6-5369-2006, 2006.

Eyring, V., Waugh, D. W., Bodeker, G. E., et al.: Multimodel projections of stratospheric ozone in the 21st century, J. Geophys. Res., 112, D16303, doi:10.1029/2006JD008332, 2007.

Eyring, V., Butchart, N., Waugh, D. W., et al.: Assessment of temperature, trace species, and ozone in chemistry-climate model simulations of the recent past, J. Geophys. Res., 111, D22308, doi:10.1029/2006JD007327, 2006.

ACPD

10, 22019–22046, 2010

Forster, P. M. de F., Bodeker, G., Schofield, R., Solomon, S., and Thompson, D: Effects of ozone cooling in the tropical lower stratosphere and upper troposphere, Geophys. Res. Lett., 34, doi:10.1029/2007GL031994, 2007.
Forster, P. M. de F. and Shine, Keith P.: Radiative forcing and temperature trends from stratospheric ozone change, J. Geophys. Res., 102, 10841–10855, 1997.
Gillett, N. P. and Thompson, D. W. J.: Simulation of recent Southern Hemisphere climate change, Science, 302, 273–275, 2003.
Hartmann, D. L., Wallace, J. M., Limpasuvan, V., Thompson, D. W. J., and Holton, J. R.: Can ozone depletion and global warming interact to produce rapid climate change? P. Natl. Acad. Sci., 97, 1412–1417, 2000.
Hu Y., Tung, K.-K., and Liu, J.: A closer comparison of early and late winter atmospheric trends in the Northern-Hemisphere, J. Climate, 18, 2924–2936, 2005.
Hu, Y. and Tung, K.-K.: Interannual and decadal variations of planetary-wave activity, stratospheric cooling, and Northern-Hemisphere Annular Mode, J. Climate, 15, 1659–1673, 2002.
Hu, Y. and Tung, K.-K.: Possible ozone induced long-term change in planetary wave activity in late winter, J. Climate, 16, 3027–3038, 2003.
IPCC: Climate Change 2007: The Physical Science Basis. Contribution of Working Group I to the Fourth Assessment Report of the Intergovernmental Panel on Climate Changes, edited by: Solomon, S., Qin, D., Manning, M., et al., Cambridge University Press, Cambridge, UK, 996 pp., 2007.
Lacis, A. A, Wuebbles, D. J., and Logan, J. A.: Radlatlve forclng of climate by changes in the vertical distrihurion nf ozone, J. Geophys. Res., 95, 9971–9981, 1990.
Meehl, G. A., Stocker, T. F., Collins, W. D., et al.: in Climate Change 2007: The Physical Science Basis. Contribution of Working Group I to the Fourth Assessment Report of the Intergovernmental Panel on Climate Change (Cambridge Univ. Press, Cambridge), 747–845, 2007.
Molnar, G. I., Ko, M. K. W., Zhou, S., and Sze, N. D.: Climatic consequences of observed ozone loss in the 1980s: Relevance to the greenhouse problem, J. Geophys. Res., 99, 25755–25760, 1994.
Perlwitz, J., Pawson, S., Fogt, R., et al.: The impact of stratospheric ozone hole recovery on Antarctic climate, Geophys. Res. Lett., 35, L08714, doi:10.1029/2008GL033317, 2008.
Ramanathan, V. and Dickinson, Robert E.: The role of stratospheric ozone in the zonal and seasonal radiative energy balance of the earth-troposphere system, J. Atmos. Sci., 36, 1084–

ACPD
10, 22019–22046, 2010

1104, 1979.
Ramaswamy, V., Schwarzkopf, M. D., and Shine, K. P.: Radiative forcing of climate from halocarbon-induced stratospheric ozone loss, Nature, 155, 810–812, 1992.
Solomon, S.: Stratospheric ozone depletion: a review of concepts and history, Rev. Geophys., 37, 275–316, 1999.
Son, S.-W., Polvani, L. M., Waugh, D. W., et al.: The Impact of Stratospheric Ozone Recovery on the Southern Hemisphere Westerly Jet, Science, 320, 1486–1489, 2008.
Son, S.-W., Tandon, N. F., Polvani, L. M., and Waugh, D. W.: Ozone hole and Southern Hemisphere climate change, Geophys. Res. Lett., 36, L15705, doi:10.1029/2009GL038671, 2009.
Son, S.-W., Polvani, L. M., Waugh, D. W., et al.: The impact of stratospheric ozone recovery on tropopause height trends, J. Climate, 22, 429–445, 2009.
Son, S.-W., Gerber, E. P., Perlwitz, J., et al.: The impact of stratospheric ozone on the southern hemisphere circulation changes: A multimodel assessment, J. Geophys. Res., submitted, 2010.
Thompson, D. W. J. and Solomon, S.: Interpretation of recent Southern Hemisphere climate change, Science, 296, 895–899, 2002.
Thompson, D. W. J. and Wallace, J. M.: Regional climate impacts of the Northern Hemisphere annular mode, Science, 293, 85–89, 2001.
Velders, G. J. M., Andersen, S. O., Daniel J. S., Fahey D. W., and McFarland M.: The importance of the Montreal Protocol in protecting climate, P. Natl. Acad. Sci., 104, 4814–4819, doi:10.1073/pnas.061032810, 2007.
Wang, W.-C., Pinto, J. P., and Yung, Y. L.: Climatic effects due to Halogenated compounds in the Earth's atmosphere, J. Atmos. Sci., 337, 333–338, 1980.
Wang, W.-C., Zhuang, Y. C., and Uojkov, R. D.: Climate implications of observed changes in ozone vertical distributions at middle and high latitudes of the northem hemisphere, Geophys. Res. Lett., 20, 1567170, doi:10.1029/93GL01318, 1991.
Weatherhead, E. C. and Andersen, S. B.: The search for signs of recovery of the ozone layer, Nature, 441, 39–45, 2006.
WMO (World Meteorological Organization): Scientific Assessment of Ozone Depletion: 2006, WMO Global Ozone Research and Monitoring Project Rep. 50, Geneva, Switzerland, 572 pp., 2007.

ACPD
10, 22019–22046, 2010

Table 1. IPCC-AR4 models used in this study. "Y" and "N" in brackets denote the model has or has not prescribed ozone recovery, respectively. Numbers indicate ensemble numbers of simulations.

Model Name	20C3M	A1B
CSIRO MK3.0	2(Y)	
CSIROMK3.5	3(Y)	1(Y)
GFDL CM2.0	3(Y)	1(Y)
GFDL CM2.1	3(Y)	1(Y)
INGV SXG	1(Y)	1(Y)
MIROC3.2 hires	1(Y)	1(Y)
MIROC3.2 medres	3(Y)	3(Y)
MPI ECHAM5/MPI-OM	4(Y)	4(Y)
NCAR CCSM3.0	8(Y)	7(Y)
NCAR PCM1	4(Y)	
UKMO HadCM3	2(Y)	1(Y)
UKMO HadGEM1	2(Y)	1(Y)
GISS EH	5(Y)	3(N)
GISS ER	9(Y)	5(N)
BCCR BCM2.0	1(N)	1(N)
CCCma CGCM3.1 T47	5(N)	5(N)
CCCma CGCM3.1 T63	1(N)	1(N)
CNRM CM3*	1(N)	1(N)
GISS AOM	2(N)	2(N)
IAP FGOALS-g1.0	3(N)	3(N)
INM CM3.0	1(N)	1(N)
IPSL CM4	2(N)	1(N)
MRI CGCM2.3.2	5(N)	5(N)

ACPD
10, 22019–22046, 2010

Table 2. CCMVal-1-1 models used in this study. REF1 and REF2 denote simulations for the 20th and 21st century, respectively. Numbers indicate ensemble numbers of simulations.

Model Name	REF1	REF2
AMTRAC	1	1
CCSRNIES		1
CMAM	1	3
GEOSCCM	1	1
MRI		1
SOCOL		1
ULAQ	1	1
WACCM	3	3

ACPD
10, 22019–22046, 2010

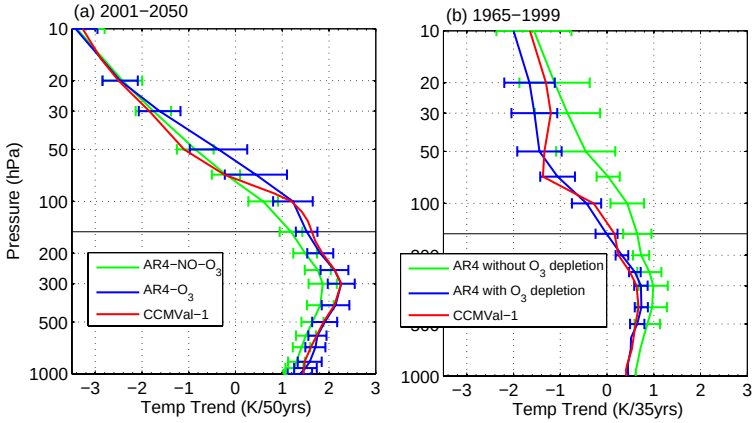

Fig. 1. Vertical profiles of global annual mean temperature trends for each ensemble-mean group for the periods of **(a)** 2001–2050 and **(b)** 1965–1999. The error bars indicate one standard deviation only for IPCC models, and error bars for CCMVal-1 models are not plotted.

ACPD
10, 22019–22046, 2010

Tropospheric temperature response to ozone recovery

Y. Hu et al.

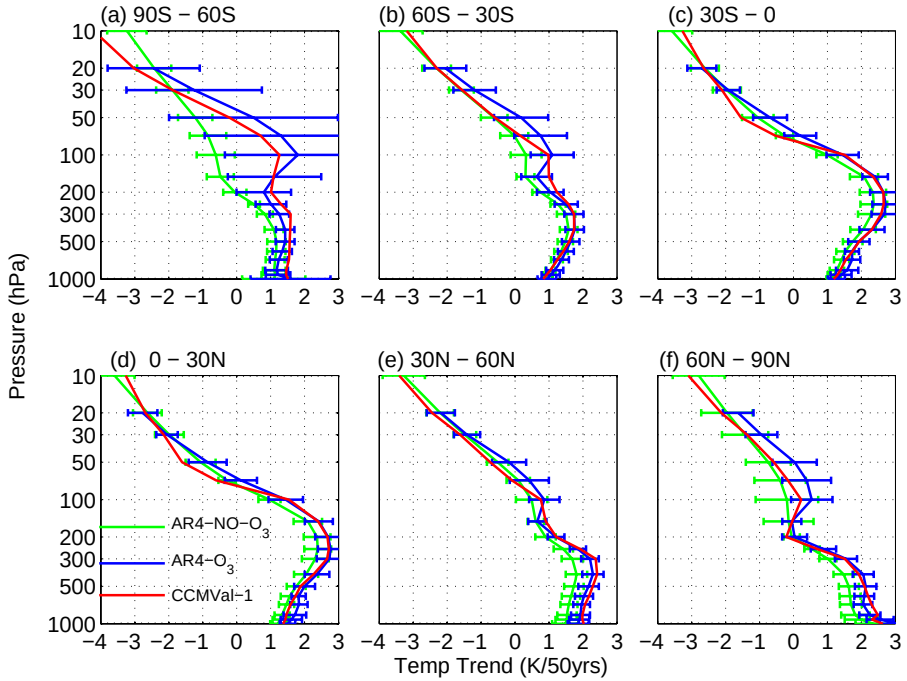

Fig. 2. Same as Fig. 1a, except for annual and regional mean temperature trends. **(a)** 90° S–60° S, **(b)** 60° S–30° S, **(c)** 30° S–0, **(d)** (a) 0–30° N, **(e)** (a) 30° N–60° N, and **(f)** 60° N–90° N.

ACPD
10, 22019–22046, 2010

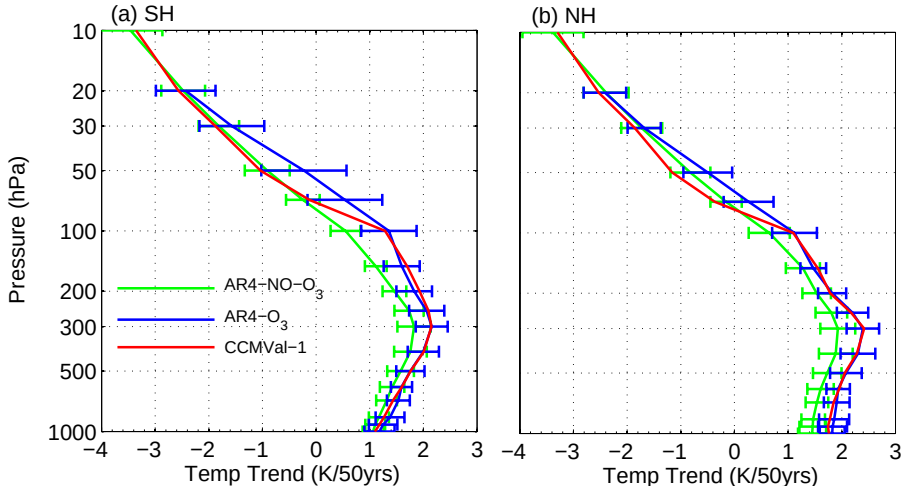

Fig. 3. Same as Fig. 1a, except for annual and hemispheric mean temperature trends. **(a)** NH, and **(b)** SH.

ACPD
10, 22019–22046, 2010

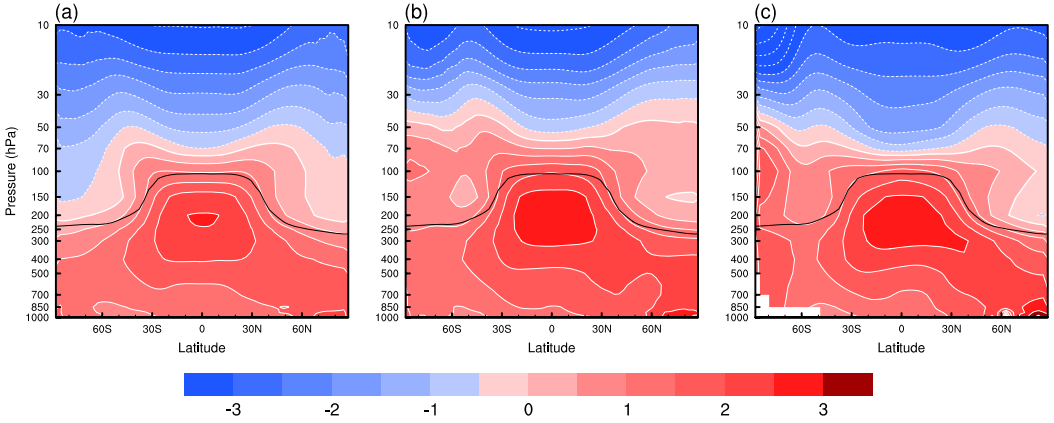

Fig. 4. Annual and zonal mean temperature trends over 2001–2050 for **(a)** AR4-O_3, **(b)** AR4-NO-O_3, and **(c)** CCMVal-1-1 models. Colour interval is 0.5 K per 50 years, pink: positive, and blue: negative. Black lines in the plots indicate the climatological positions of the tropopause.

ACPD
10, 22019–22046, 2010

Tropospheric temperature response to ozone recovery

Y. Hu et al.

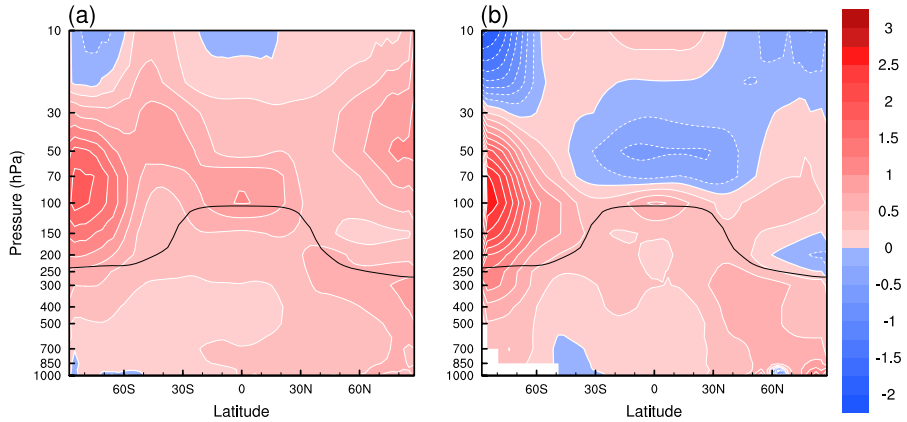

Fig. 5. Differences of annual and zonal mean temperature trends over 2001–2050 **(a)** between AR4-O_3 and AR4-NO-O_3 models, and **(b)** between CCMVal-1 and AR4-NO-O_3 models. Color interval is 0.25 K per 50 years, pink: positive, and blue: negative. Black lines in the plots indicate the climatological position of the tropopause.

ACPD
10, 22019–22046, 2010

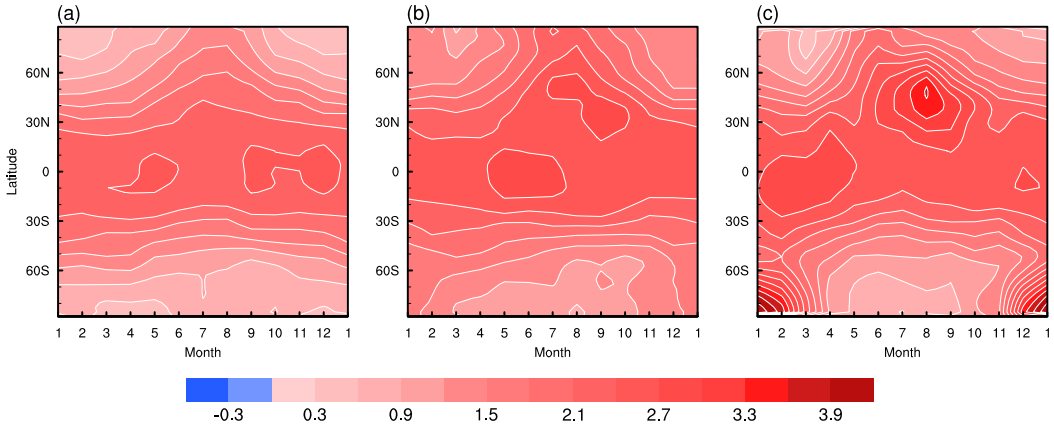

Fig. 6. Latitude-month plots of zonal-mean temperature trends at 300 hPa over 2001–2050. **(a)** AR4-NO-O_3, **(b)** AR4-O_3, and **(c)** CCMVal-1 models. Colour interval is 0.30 K per 50 years.

ACPD
10, 22019–22046, 2010

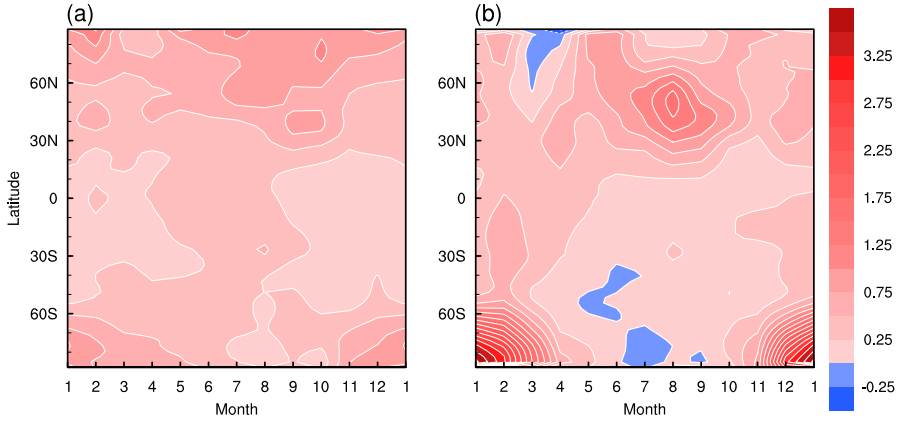

Fig. 7. Latitude-month plots of zonal-mean temperature trend differences at 300 hPa over 2001–2050. **(a)** Difference between AR4-O_3 and AR4-NO-O_3 models, and **(b)** difference between CCMVal-1 and AR4-NO-O_3 models. Colour interval is 0.25 K per 50 years, pink: positive, and blue: negative.

ACPD
10, 22019–22046, 2010

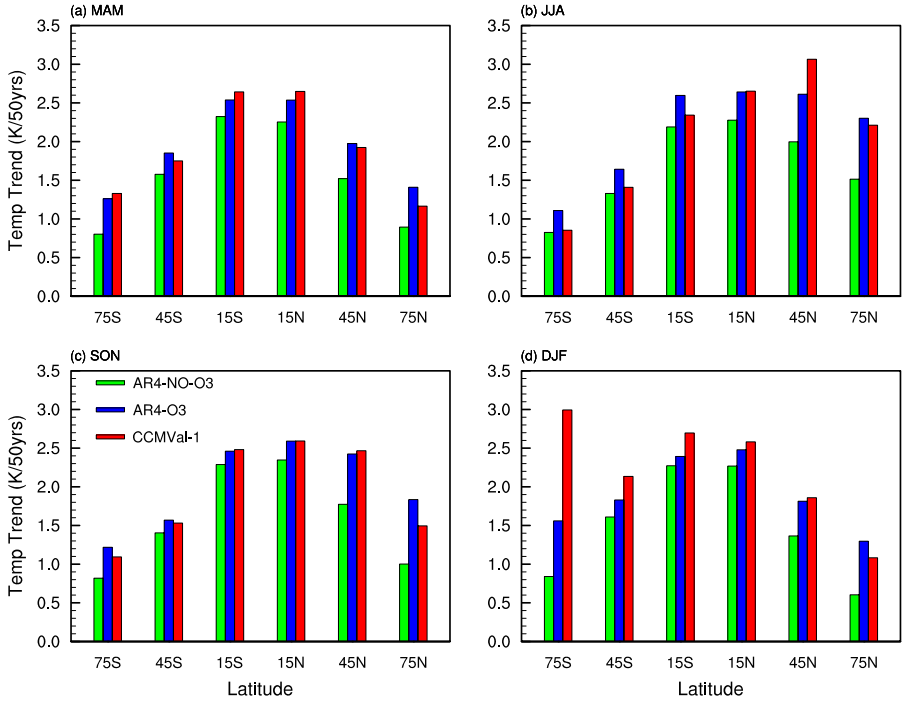

Fig. 8. Comparison of zonal-mean temperature trends at 300 hPa by latitude over 2001–2050. **(a)** MAM, **(b)** JJA, **(c)** SON, and **(d)** DJF.

ACPD
10, 22019–22046, 2010

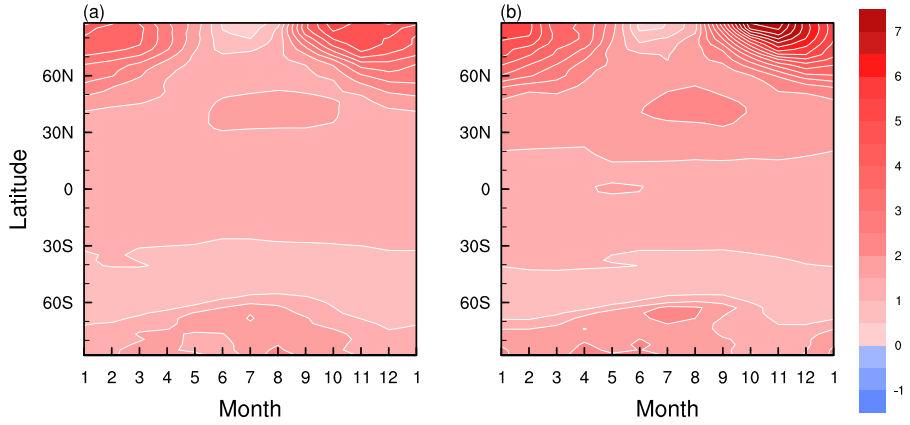

Fig. 9. Latitude-month plots of zonal-mean SAT trends for AR4 models. **(a)** AR4-NO-O_3 models, and **(b)** AR4-O_3 models. Colour interval is 0.50 K per 50 years, pink: positive, and blue: negative.

ACPD
10, 22019–22046, 2010

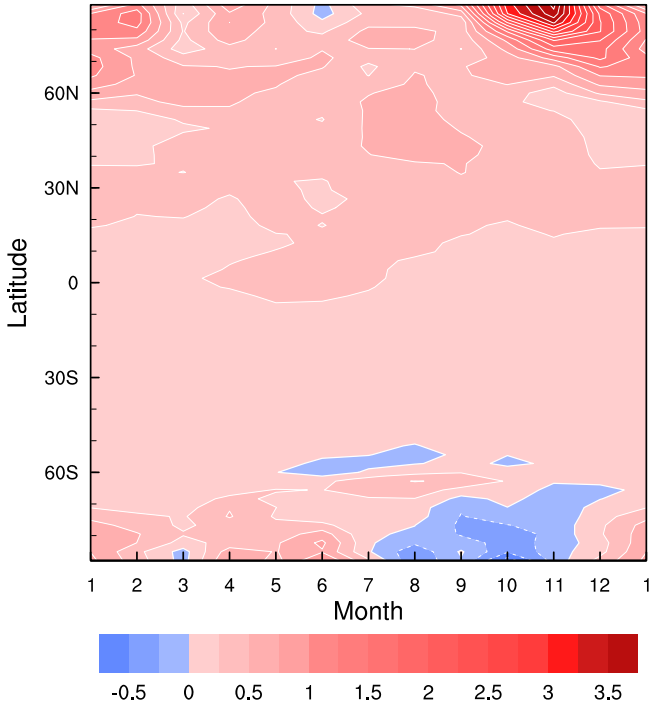

Fig. 10. Latitude-month plots of zonal-mean SAT trend differences between AR4-O_3 and AR4-NO-O_3 models over 2001–2050. Colour interval is 0.25 K per 50 years, pink: positive, and blue: negative.

ACPD
10, 22019–22046, 2010